Serkan Abali* and Ahmet Ekerim

Mechanical Properties of the Directionally Solidified Ceramic Eutectic of $Al_2O_3/Al_{16}Ti_5O_{34}$ Phase Structure

Abstract: Al_2O_3/TiO_2 eutectics containing 62–64 wt% Al_2O_3 were fabricated by a laser floating zone method. Raman spectrometry was used to determine the phase composition. The compressive creep strength of AT36 ($Al_{16}Ti_5O_{34}/Al_2O_3$) crystal at 1500°C under the strain rate of 1.0×10^{-4} s^{-1} has 372 MPa, which is about higher than β-Al_2TiO_5 and β-Al_2TiO_5/Al_2O_3 crystals. High-temperature flexural strength, elastic modulus, hardness and fracture toughness of the AT36 crystals were analyzed. The highest flexure strength at ambient temperature was found in the material with 36 wt% TiO_2. In addition, we briefly discussed the relationships between microstructure and mechanical properties in AT36 crystal.

Keywords: alumina, rutile, strength, eutectic, aluminum titanate

PACS® (2010). 81.05.Je, 81.10.Fq, 81.30.Fb, 81.40.Gh

***Corresponding author: Serkan Abali:** Çanakkale Onsekiz Mart University, Çan Vocational School, Department of Materials and Materials Processing Technology, Çanakkale 17400, Turkey
E-mail: sabali@comu.edu.tr
Ahmet Ekerim: Yildiz Technical University, Faculty of Chemical and Metallurgical Engineering, Department of Metallurgical and Materials, Istanbul 34210, Turkey

1 Introduction

Alumina and aluminum titanate polycrystals (AT) are ceramics showing considerable promise for use in a number of engineering applications [1]. Nevertheless, these materials have been limited by low toughness and thermal shock resistance for alumina, and low mechanical strength at high temperatures [2]. However, sapphire single crystals (Al_2O_3 single crystals) maintain their physical properties up to 600°C. In the advanced power generator field, studies all over the world are seeking to develop ultra-high-temperature structural materials that will improve thermal efficiency in aircraft engines and high-efficiency gas turbines [3]. Previous studies have shown that creep behavior of eutectic crystal better than sapphire crystal [4]. Research is being vigorously pursued into the development of ultra-high-temperature structural materials that remain stable under use for prolonged periods in an oxidizing atmosphere at temperatures above 1650°C. These materials must be suitable for use as non-cooled turbine blades. Such materials must offer a performance balance in such areas as high-temperature strength, oxidation resistance, creep resistance, fatigue resistance, thermal shock characteristics, and fracture toughness [5] and [6].

Single crystal composite eutectic oxide ceramics are important materials because they have superior properties, such as high bending and creep strengths [7], [8] and [9]. The mechanical properties of single-crystal oxides are dictated by the ionic bonding between the atoms and by the peculiar characteristics of the eutectic microstructure, which shares many similarities with single-crystal oxides and ceramic composites. Ionic bonding leads to hard and brittle materials with high elastic modulus and high melting point, and where plastic deformation is impeded up to very high temperature [10]. Previous studies [11], [12], [13] and [14] have shown that oxides like alumina/aluminum titanate, rutile are solidified with the laser heated float zone and that eutectic ceramics such as Al_2O_3/Y_2O_3 and $Al_2O_3/Y_2O_3/ZrO_2$ are formed into single crystals with directionally solidification methods [15], [16], [17], [18] and [19]. Moore also reported that TiO_2 is easily dissolved into Al_2O_3 during single crystal formation [20]. Fracture toughness of eutectic single crystals decreases due to thermal expansion mismatch between two phases [21]. Previous studies have indicated that alumina/aluminum titanate structure has a high potential for eutectic composites that combine strength and flaw tolerance [22].

Hoffmann conducted that the stoichiometry of the new compound $Al_{16}Ti_5O_{34}$ was calculated mol% 8 $Al_2O_3 \times 5\ TiO_2 = 61.5\%\ Al_2O_3 : 38.5\%\ TiO_2$. Graphical representation in Figure 1 has determined the composition of $Al_{16}Ti_5O_{34}$ [23]. The proposed structure of new $Al_{16}Ti_5O_{34}/Al_2O_3$ phase was confirmed by the Raman analysis. Accordingly, to

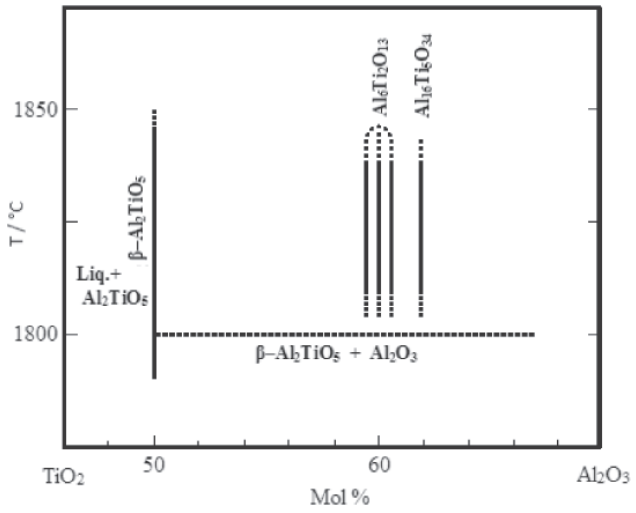

Fig. 1: Graphical representation of the experimental findings for the investigated compositional range in the system Al_2O_3/TiO_2 [23].

investigate the possibilities of $Al_{16}Ti_5O_{34}/Al_2O_3$ compound as a very high temperature-resistant structural material, this research evaluated its major creep characteristics, microstructural features, elastic modulus and flexural strength at high temperatures.

2 Experimental

Using commercially available Al_2O_3 powder (Kale Ceramic Co., purity 99.99%) and TiO_2 (consisting of 95 wt% rutile and 5 wt% anatase according to X-ray powder pattern, Kale Mining Co.) powder wet ball milling of a Al_2O_3/TiO_2 (62/38, 63/37 and 64/36 wt%) was undertaken to obtain an uniform composite powder slurry. The slurry obtained was fired (at 1000°C throughout 1 h), milled in an agate mortar and sieved (0.3 μm). Precursor rods (1–2 mm in diameter and 50–100 mm length) were made by isostatic pressing of the mix powder at 300 MPa, followed by sintering at 1400°C. Eutectic single crystals were obtained by the directional solidification method using the laser heated floating zone technique with a growth rate of 250 mm/min.

The Raman patterns obtained from Raman active materials provide information similar to other spectroscopic techniques in that the pattern is unique to that specific material [24]. Much has been done to study single crystal microstructure by the latest method Raman spectroscopic technique (Confocal laser Raman and photoluminescence micro spectrometer) in modeling to provide an ever more precise phase characterization of single crystals microstructures.

Creep tests were carried out on the 3 mm × 4 mm × 20 mm specimens. The specimens used in the creep test were selected so that its axial direction was parallel to the solidification direction. The rods were dead weight loaded at temperature using cold grips in high vacuum (10^{-1} Pa) at 1500°C in a tungsten element furnace. Creep tests were conducted under constant load mode. Because small creep strains (~1%) were expected the conditions amounted to constant stress.

The strength of the rods in the longitudinal direction was measured from 27 to 1000°C by flexure tests carried out in an alumina three-point bend testing fixture of 8.5 mm loading span. The specimen and the loading fixture were placed in a furnace and loaded through two alumina rods connected to the actuator and load cell, respectively, of a servo-mechanical testing machine (model 4505, Instron Ltd.). The specimen was held at the test temperature for 30 min before testing. The tests were performed in air under stroke control at a cross-head speed of 50 μm/min. The flexure strength was computed from the maximum load in the test according to the strength of materials theory for an elastic beam of circular section.

Young's modulus was calculated using the Marshall and Evans equation (see Eq. (1)) from of the size of indentation tracks obtained applying a 5 N load during 15 s with a Knoop indenter. This equation is based on elastic energy recuperation produced in the coating after removing the Knoop indenter [26] and [27].

$$E = \frac{-\alpha H}{\frac{b'}{a'} - \frac{b}{a}} \tag{1}$$

α is a constant ($\alpha = 0.45$), H is the Knoop hardness (Pa); a' and b' are the longer and shorter diagonals respectively produced by indentation (μm); a and b are geometric constants of the indenter ($b/a = 1/7.11$).

The toughness was calculated from radial cracks and indentation tracks, produced by the application of a 3 N load during 15 s with a Vickers indenter, and using Eq. (2) [28] and [29]. The load applied was determined on the criteria $C > 2a$ without chipping of crystal.

$$K_{IC} = 0.0016\sqrt{\frac{E}{H}}\frac{P}{(C)^{3/2}} \tag{2}$$

where K_{IC} is the toughness of the crystal (MPam$^{1/2}$), C is the length of the longest radial crack (mm) produced by the load applied, E is Young's modulus (GPa), H is the Vickers hardness of the crystal (GPa), P is the load applied by the

indenter (N) and in the criteria $C > 2a$, a is the half diagonal of the indentation track (mm).

Microstructural characterization was carried out by using scanning electron microscopy (SEM) techniques. The SEM images were obtained on a JEOL JSM-6335F microscope. Observation of the interface of the Al_2O_3 and the $Al_{16}Ti_5O_{34}$ phases was carried out using a high-resolution transmission electron microscopy (JEOL JEM-2010).

Some of the mixed powder material (Al_2O_3–TiO_2) with 36 wt% TiO_2 was prepared by isostatically pressing the powder for ~2 min at 200 MPa. The compacts fired for ~12 h at 1500°C in vacuum to fabricate a sintered $Al_{16}Ti_5O_{34}$/Al_2O_3 composite of dimensions 40 mm × 60 mm × 5 mm.

3 Results and discussion

3.1 Phase composition

Raman spectra of the oriented single crystals identified optically are shown in Fig. 2. A total of four bands (Al_2O_3, β-Al_2TiO_5/Al_2O_3, $Al_{16}Ti_5O_{34}$/Al_2O_3, β-Al_2TiO_5) are observed in these polarized single-crystal spectra. For the identification of the crystallographic phases used micro Raman dispersion spectra. Fig. 2 shows the mineral analysis of the $Al_{16}Ti_5O_{34}$/Al_2O_3 (AT36), β-Al_2TiO_5 (AT37), β-Al_2TiO_5/Al_2O_3 (AT38) single crystals. AT36 phase compositions were determined using the one sharp peak obtained at 574 cm^{-1} wavelength. The sharp, intense peak confirms the quality of the AT36 phase. The broad and asymmetric nature of this peak is typical of the Raman active mode specially observed from the aluminum titanate structure. The spectrum is dominated by the presence of a strong peak located at 574 cm^{-1}. Increasing the amount of the TiO_2 phase the AT37 and AT38 respectively, crystals gave peaks at 611 cm^{-1} and 638 cm^{-1} obtained wavelength with an intensity lower than that of the remaining. The Raman spectrum of the as AT37 sample shows a broad hump at 611 cm^{-1}. However AT38 compositions were observed at several prominent peaks, their intensities lower than AT36 phase.

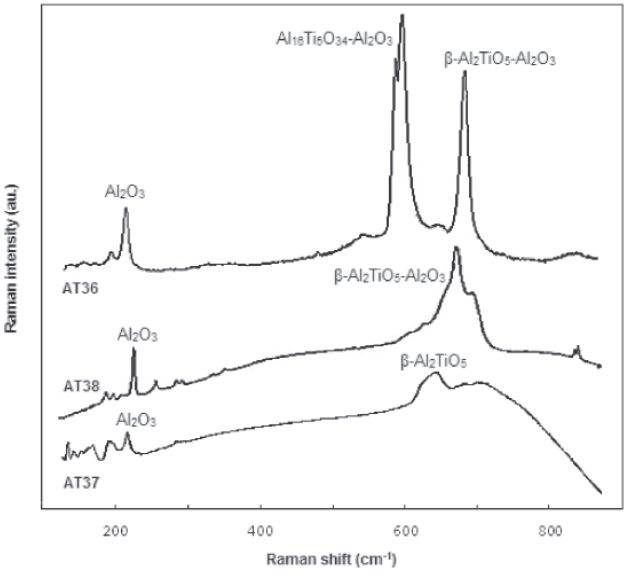

Fig. 2: Raman spectra of AT36, AT37 and AT38 phases. The most intense peak was found to be at approximately 574 cm^{-1} in these compounds, i.e., 611 cm^{-1} for AT37, and 638 cm^{-1} for AT38, respectively.

3.2 Mechanical behavior

Fig. 3 shows the relationship between compressed creep stress and strain rate in AT36, AT37 and AT38 eutectic composites at test temperature of 1500°C. Diffusion process has a critical role in steady state creep process of sapphire. If the diffusion process can be slowed down to some extends with proper doing, such as Ti^{4+}, the steady state creep strain rate will be reduced correspondingly [30]. As can be seen from the diagram, the AT36 crystal eutectic has creep characteristics that surpass those of c-axis AT37 and AT38 displays excellent creep resistance. Using the secondary phase particles, hardening mechanism of dislocation movement was blocked. That's the most important factor affecting the strength of creep, thermal stability and inter-crystalline phases, with the balance of the main structure. The interfacial bonding of $Al_{16}Ti_5O_{34}$ crystal is further increased in many oxide eutectic systems by the presence of homopolar surfaces, where

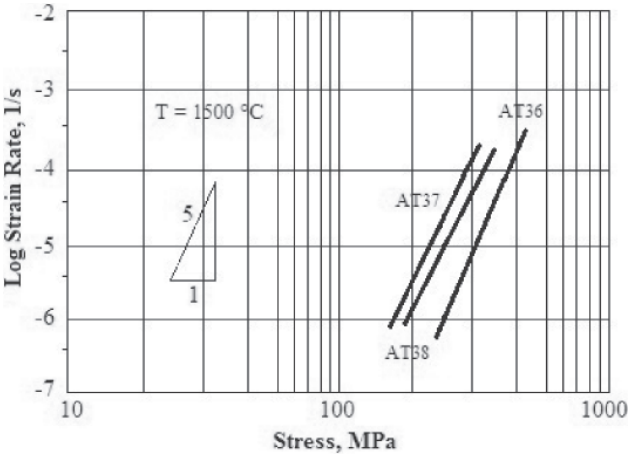

Fig. 3: Comparison of compression creep in AT36, AT37 and AT38 eutectic composites.

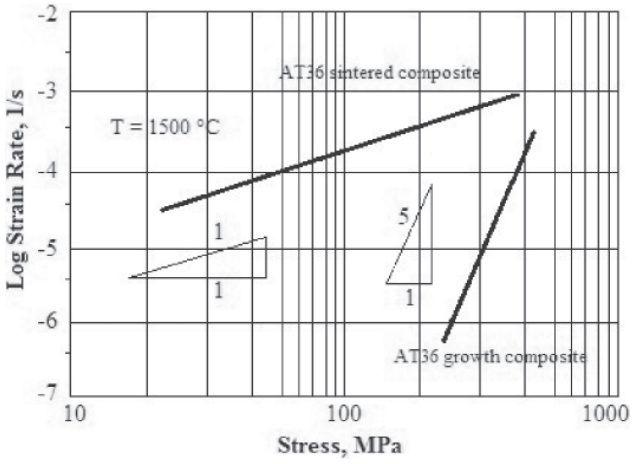

Fig. 4: Comparison of compression creep in a AT36 solidified eutectic composite and sintered composite with the same chemical composition.

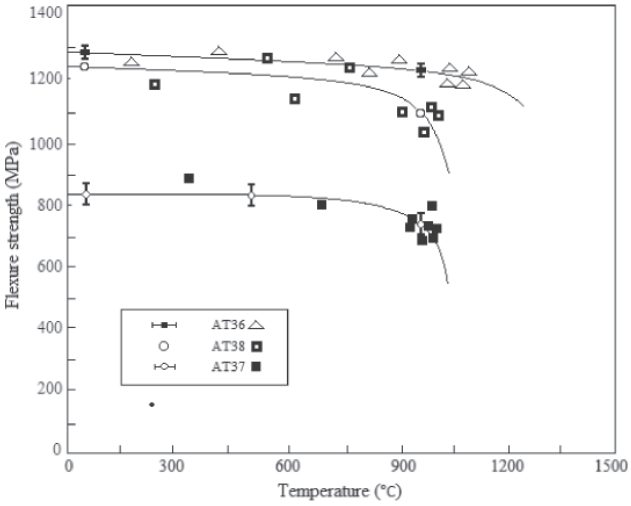

Fig. 5: High temperature flexure strength of AT36, AT37 and AT38 eutectics. Eutectic rods processed by the laser floating zone method were tested in three point bending.

they share a common oxygen plane. This leads to electrostatic bonding across the boundary, which retains the strength even at very high temperature. In the absence of relative sliding at the domain boundaries, compatibility of deformation between the eutectic phases is compulsory, and the overall strain rate is controlled by the eutectic morphology and the creep resistance of both phases [10]. Fig. 4 shows the relationship between compressed creep stress and strain rate in a AT36 eutectic composite at test temperature of 1500°C and a sintered composite at 1500°C. AT36 grown crystal and the sintered composite shared the same chemical composition, but their creep characteristics were markedly different. Conventionally sintered oxide and non-oxide polycrystalline ceramics always present a glassy phase at the grain boundaries, and high temperature deformation occurs by grain boundary sliding, as opposed to the dislocation motion in single crystal eutectics [31].

The effect of the temperature on the longitudinal strength of the AT36, AT37 and AT38 eutectics was ascertained through three-point bending tests at 1000°C. Fig. 5 shows the AT36 eutectics presented good strength retention up to 900°C. AT36 retained the ambient temperature strength up to 1000°C because the domain boundary of AT36 single crystal was free of amorphous phases and the resistance to deformation was controlled by the activation of plastic slip. Fig. 6 shows typical high-resolution transmission electron microscope image of the interfaces between $Al_{16}Ti_5O_{34}$ and Al_2O_3 phases in the $Al_{16}Ti_5O_{34}/Al_2O_3$ eutectic structure. Domain boundaries in the eutectics act as barriers to dislocation motion at high temperature and can improve the resistance to plastic deformation. Amount of plastic deformation in this regime is very sensitive to

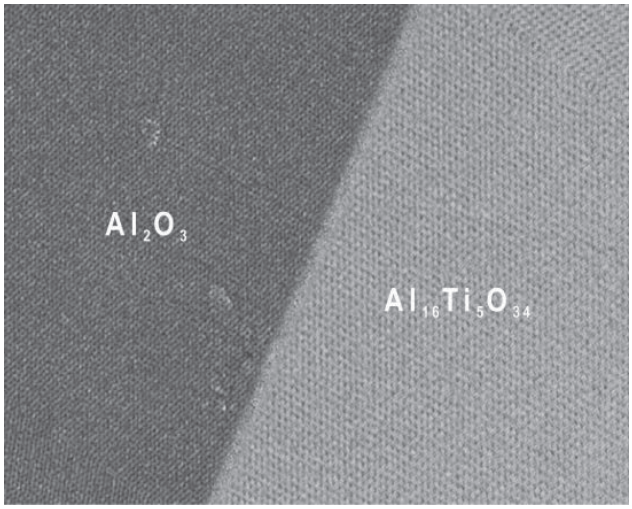

Fig. 6: HRTEM image of the grain boundary between Al_2O_3 and $Al_{16}Ti_5O_{34}$ phases of a directionally solidified eutectic structure.

the strain rate and to the domain size, and the ductile/brittle transition temperature depends on both factors [32]. However, the strength gradually dropped above this temperature: for instance, the flexure strength at 1200°C decreased by only ~20% compared with the ambient temperature.

This degradation in strength was attributed to several factors, including the release of residual stresses, the plastic deformation of TiO_2 and the proximity of the eutectic temperature. Furthermore, microcracks across the interdendrite phase associated with crack deflection along the alumina dendrites are responsible for the strain

Crystal	Mechanical properties		
	HV (GPa)	*E* (GPa)	K_{IC} (MPa m$^{1/2}$)
AT36	9.1 ± 1.2	157.2 ± 46.0	4.3 ± 1.4
AT37	7.8 ± 0.3	164.3 ± 21.9	4.4 ± 0.2
AT38	11.6 ± 0.8	94.0 ± 42.1	3.1 ± 0.2

Table 1: Mechanical properties of crystals

capabilities of these off-eutectic compositions. The load-bearing constituents in the material directionally solidified at the eutectic composition are eutectic colonies of the same crystallographic orientation. For the specimens solidified at the eutectic composition, crack deflection along colony interfaces is responsible for the graceful fracture and the associated increase in strain capability [21]. Previous studies have reported [11] the crack deflection occurs at the boundaries of the Al_2O_3 dendrites that are microcracked. The arms of the dendrites provide additional interlocking between dendrites to carry the load cooperatively through load sharing.

3.3 Elastic modulus, fracture toughness and hardness

The mechanical properties of eutectic crystals are presented in Table 1. Results obtained indicate that AT37 crystals have better fracture toughness than AT38 and AT36. However, three compositions (AT36, AT37 and AT38) show similar results to each other. Additionally AT36 crystal have higher Young's modulus than those of AT38, which is due to the higher Young's modulus of Al_2O_3 compared with that of aluminum titanates (Al_2TiO_5 and Al_6TiO_2) [34].

3.4 Microstructure

Fig. 7 is a SEM photograph of the cross-section perpendicular to the solidified AT36 eutectic crystal. The white and black regions correspond to the $Al_{16}Ti_5O_{34}$ and Al_2O_3 phases, respectively. At the macroscopic level, the solidified eutectic structure has a uniform microstructure with no colonies or pores. The existence of amorphous phases at microstructure leads to a reduction in the mechanical properties of the materials at high temperature but for the single crystals, no amorphous phases are observed at the microstructure between the two phases [6].

As shown in Fig. 8, which shows the results of observing the cross-section microstructure after the creep testing, in the solidified AT36 crystal, no defects can be

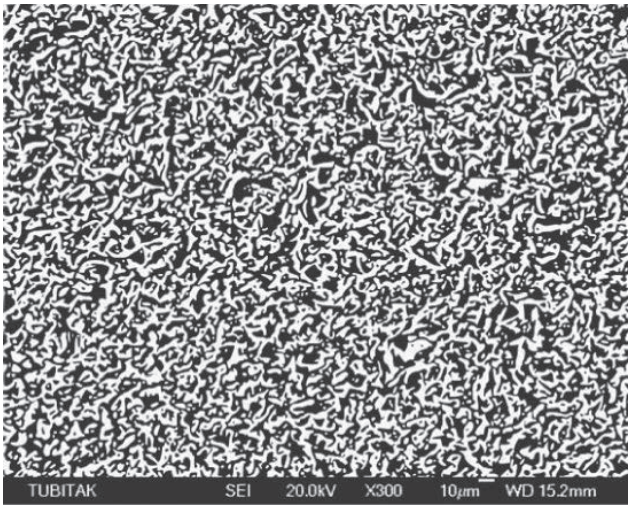

Fig. 7: SEM image of cross-sections of sample AT36: distances between dendrites are short in the sample consist of Al_2O_3 (dark phase) and $Al_{16}Ti_5O_{34}$ (bright phase).

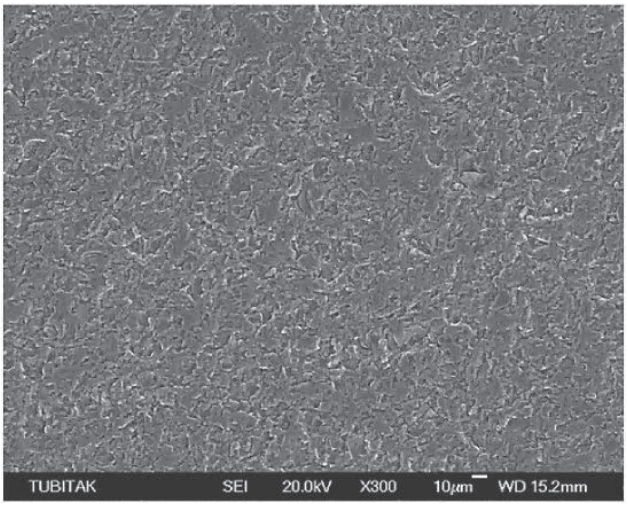

Fig. 8: A SEM photograph showing fracture surfaces in creep tested specimens at 1500°C of the AT36 single crystal system.

observed in the microstructure. AT36 single crystal structure has not been observed amorphous phase. Fig. 9 is a SEM image of the fracture surface of AT36 sintered composite after the creep testing. In sintered AT36 structure, the domain boundaries are located in the amorphous phases that are responsible for the strength reduction. Fig. 10 shows the microstructure of cross-section perpendicular to the solidification direction of AT36 after crept test at 1500°C. AT36 microstructure shows no grain growth up to the very high temperature of 1500°C. Interfacial properties of eutectic structure has a significant impact that the creation of this microstructure.

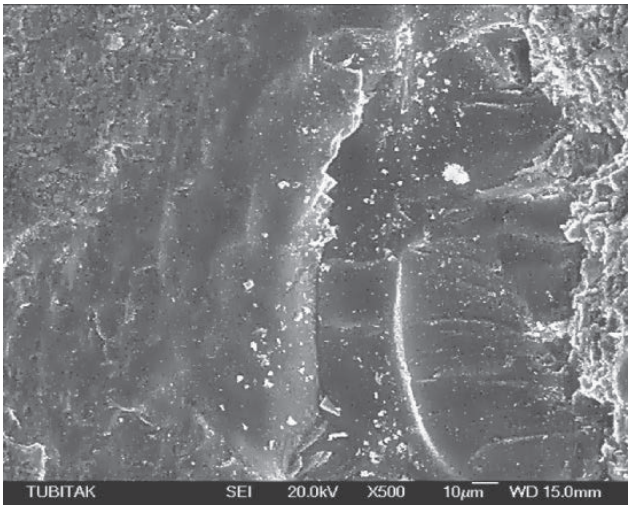

Fig. 9: A SEM photograph showing fracture surfaces in creep tested specimens at 1500°C of the AT36 sintered composite.

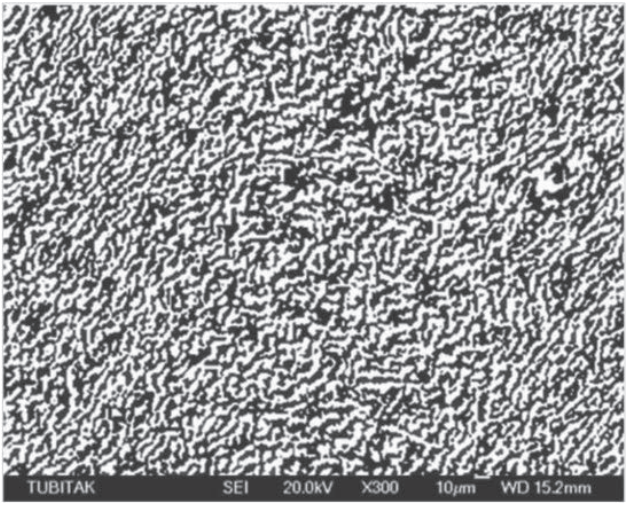

Fig. 10: SEM image showing microstructural change of cross-section perpendicular to the solidification of AT36 after creep test at 1500°C.

4 Conclusion

$Al_{16}Ti_5O_{34}/Al_2O_3$ eutectic crystals with good mechanical behaviors have been fabricated successfully by using laser heated floating zone process of the Al_2O_3/TiO_2 powders. AT36 crystal has a very thermally stable microstructure with no amorphous phase in evidence after lengthy heat treatment at a high temperature of 1500°C. Creep resistance of AT36 was higher than AT37 and AT38 structures and sintered composite with the same chemical composition. In addition, this structure has excellent high temperature strength showing no temperature dependence in the range from room temperature up to 900°C. AT36 crystal had a lower microhardness than AT38 crystal. But it had higher elastic modulus and toughness than AT38 structure. AT36 crystal has optimal hardness, toughness and elasticity properties. AT36 new phase structure can improve the properties of the alumina matrix.

Acknowledgements: This study was supported by TUBITAK (The Scientific and Technological Research Council of Turkey) in terms of technical information for material analysis.

Received: August 4, 2012. Accepted: November 16, 2012.

References

[1] S. Pratapa, I.M. Low, B.H. O'Connor, Infiltration-processed, functionally graded aluminum titanate/zirconia–alumina composite, Part I: Microstructural characterization and physical properties, Journal of Materials Science, 33 (1998) 3037–3045.

[2] M. Ishitsuka, T. Sato, T. Endo, M. Shimada, Synthesis and thermal stability of aluminum titanate solid solutions, Journal of the American Ceramic Society, 70 (1987) 69–71.

[3] Y. Waku, N. Nakagawa, T. Wakamoto, H. Ohtsubo, K. Shimizu, Y. Kohtoku, High–temperature strength and thermal stability of a unidirectionally solidified Al_2O_3/YAG eutectic composite, Journal of Materials Science 33 (1998) 1217–1225.

[4] A. Sayir, S.C. Farmer, The effect of the microstructure on mechanical properties of directionally solidified Al_2O_3/$ZrO_2(Y_2O_3)$ eutectic, Acta Materialia, 48 (2000) 4691–4697.

[5] E.L. Courtright, H.C. Graham, A.P. Katz, R.J. Kerans, Ultrahigh temperature assessment study: ceramic matrix composites, Report number: WL-TR-91–4061, Wright Laboratory, Wright Patterson Air Force Base, OH, 1992.

[6] Y. Waku, N. Nakagawa, T. Wakamoto, H. Ohtsubo, K. Shimizu, Y. Kohtoku, The creep and thermal stability characteristics of a unidirectionally solidified Al_2O_3/YAG eutectic composite, Journal of Materials Science, 33 (1998) 4943–4951.

[7] Y. Waku, N. Nakagawa, T. Wakamoto, H. Ohtsubo, K. Shimizu, Y. Kohtoku, A ductile ceramic eutectic composite with high-strength at 1,873 K, Nature, 389 (1997) 49–52.

[8] D. Viechnicki, F. Schmid, Eutectic solidification in the system $Al_2O_3/Y_3Al_5O_{12}$, Journal of Materials Science 4 (1969) 84–88.

[9] F.L. Kennard, R.C. Bradt, V.S. Stubican, Mechanical properties of the directionally solidified MgO–$MgAl_2O_4$ eutectic, Journal of the American Ceramic Society, 59 (1976) 160–163.

[10] J. LLorca, V.M. Orera, Directionally solidified eutectic ceramic oxides, Progress in Materials Science, 51 (2006) 711–809.

[11] A. Sayir, M.H. Berger, C. Baudin, Microstructural and mechanical properties of directionally solidified ceramic in Al_2O_3–Al_2TiO_5 system, in: E. Lara-Curzio (Eds.), Mechanical Properties and Performance of Engineering Ceramics and Composites: Ceramic Engineering and Science Proceedings, John Wiley & Sons Inc., Hoboken, NJ, USA, 2005, pp. 225–233.

[12] C. Baudin, A. Sayir, M.H. Berger, Failure mechanisms in directionally solidified alumina–titania composites, Key Engineering Materials, 290 (2005) 199–202.
[13] T. Kotani, H.L. Tuller, Growth of TiO_2 single crystals and bicrystals by the laser-heated floating-zone method, Journal of the American Ceramic Society, 81 (1998) 592–596.
[14] M. Higuchi, T. Hosokawa, Growth of rutile single crystals by floating zone method, Journal of Crystal Growth, 112 (1991) 354–358.
[15] Y. Waku, H. Ohtsubo, N. Nakagawa, Y. Kohtoku, Sapphire matrix composites reinforced with single crystal YAG phases, Journal of Materials Science, 31 (1996) 4663–4670.
[16] Y. Waku, N. Nakagawa, H. Ohtsubo, A. Mitani, K. Shimizu, Fracture and deformation behavior of melt growth composites at very high temperatures, Journal of Materials Science, 36 (2001) 1585–1594.
[17] Y. Waku, S. Sakata, A. Mitani, K. Shimizu, M. Hasebe, Temperature dependence of flexural strength and microstructure of $Al_2O_3/Y_3Al_5O_{12}/ZrO_2$ ternary melt growth composites, Journal of Materials Science, 37 (2002) 2975–2982.
[18] J.I. Peña, M. Larsson, R.I. Merino, I. de Francisco, V.M. Orera, J. LLorca, J.Y. Pastor, A. Martín, J. Segurado, Processing, microstructure and mechanical properties of directionally-solidified Al_2O_3–$Y_3Al_5O_{12}$–ZrO_2 ternary eutectics, Journal of the European Ceramic Society 26 (2006) 3113–3121.
[19] J.H. Lee, A. Yoshikawa, H. Kaiden, K. Lebbou, T. Fukuda, D.H. Yoon, Y. Waku, Microstructure of Y_2O_3 doped Al_2O_3/ZrO_2 eutectic fibers grown by the micro-pulling-down method, Journal of Crystal Growth, 231 (2001) 179–185.
[20] C.H. Moore, Formation and properties of single crystals of synthetic rutile, Transactions of the American Institute of Mining, Metallurgical and Petroleum Engineers, 184 (1949) 194.
[21] C. Baudin, A. Sayir, M.H. Berger, Mechanical behavior of directionally solidified alumina/aluminum titanate ceramics, Acta Materialia, 54 (2006) 3835–3841.
[22] N.P. Padture, S.J. Bennison, J.L. Runyan, J. Rödel, H.M. Chan, B.R. Lawn, Flaw tolerant Al_2O_3–Al_2TiO_5 composites, Ceramic Transactions, 19 (1991) 715–721.
[23] S. Hoffmann, S.T. Norberg, M. Yoshimura, Structural models for intergrowth structures in the phase system Al_2O_3–TiO_2, Journal of Solid State Chemistry, 178 (2005) 2897–2906.
[24] J. Liu, Y.K. Vohra, Raman modes of 6H polytype of silicon carbide to ultrahigh pressures: A comparison with silicon and diamond, Physical Review Letters, 72 (1994) 4105–4108.
[25] Y. Waku, H. Yasuda, High temperature characteristics of unidirectionally solidified eutectic ceramic composites and some potential applications, Materials Science Forum, 997 (2010) 638–642.
[26] D.B. Marshall, T. Noma, A.G. Evans, Controlled flaws in ceramics: A comparison of Knoop and Vickers indentation, Journal of the American Ceramic Society, 66 (1983) 127–131.
[27] R.S. Lima, S.E. Kruger, G. Lamouche, B.R. Marple, Elastic modulus measurements via laser-ultrasonic and Knoop indentation techniques in thermally sprayed coatings, Journal of Thermal Spray Technology, 14 (2005) 52–60.
[28] T. Scholz, G.A. Schneider, J. Munoz-Saldana, M.V. Swain, Fracture toughness from submicron derived indentation cracks, Applied Phyics Letters, 84 (2004) 3055–3057.
[29] I.J. McColm, Ceramic Hardness, 1st ed., Plenum Press, New York, 1990.
[30] J. Yi, Creep resistance of directionally solidified eutectic ceramics: experiments and model, Ph.D. thesis, Department of Mechanical Engineering, Massachusetts Institute of Technology, Cambridge, MA, USA, 2004.
[31] T. Mah, T.A. Parthasarathy, L.E. Matson, Processing and mechanical properties of $Al_2O_3/Y_3Al_5O_{12}$ (YAG) eutectic composite, in: J.B. Wachtman (Eds.), 14th Annual Conference on Composites and Advanced Ceramic Materials: Ceramic Engineering and Science Proceedings, John Wiley & Sons Inc., Hoboken, NJ, USA, 1990, pp. 1617–1627.
[32] S. Ochiai, Y. Sakai, K. Sato, Fracture characteristics of Al_2O_3/YAG composite at room temperature to 2023 K, Journal of the European Ceramic Society, 25 (2005) 1241–1249.
[33] M.H. Berger, A. Sayir, Directional solidification of Al_2O_3–Al_2TiO_5 system, Journal of the European Ceramic Society, 28 (2008) 2411–2419.